



UNIVERSITY OF LEEDS

This is a repository copy of *Optimization of Standing-Wave Thermoacoustic Refrigerator Stack Using Genetic Algorithm*.

White Rose Research Online URL for this paper:
<http://eprints.whiterose.ac.uk/132121/>

Version: Accepted Version

Article:

Peng, Y, Feng, H and Mao, X orcid.org/0000-0002-9004-2081 (2018) Optimization of Standing-Wave Thermoacoustic Refrigerator Stack Using Genetic Algorithm. *International Journal of Refrigeration*, 92. pp. 246-255. ISSN 0140-7007

<https://doi.org/10.1016/j.ijrefrig.2018.04.023>

(c) 2018, Elsevier Ltd and IIR. This manuscript version is made available under the CC BY-NC-ND 4.0 license <https://creativecommons.org/licenses/by-nc-nd/4.0/>

Reuse

This article is distributed under the terms of the Creative Commons Attribution-NonCommercial-NoDerivs (CC BY-NC-ND) licence. This licence only allows you to download this work and share it with others as long as you credit the authors, but you can't change the article in any way or use it commercially. More information and the full terms of the licence here: <https://creativecommons.org/licenses/>

Takedown

If you consider content in White Rose Research Online to be in breach of UK law, please notify us by emailing eprints@whiterose.ac.uk including the URL of the record and the reason for the withdrawal request.



eprints@whiterose.ac.uk
<https://eprints.whiterose.ac.uk/>

Optimization of Standing-Wave Thermoacoustic Refrigerator Stack Using Genetic Algorithm

Yehui Peng^{*1}, Heying Feng², Xiaoan Mao³

¹ School of Mathematics and Computational Science, Hunan University of Science and Technology, Xiangtan, Hunan, China, 411201, email: pengyehui@hnust.edu.cn

² Hunan Provincial Key Laboratory of Health Maintenance for Mechanical Equipment, Hunan University of Science and Technology, Xiangtan, Hunan, China, 411201, email: fengheyings@hnust.edu.cn

³ Faculty of Engineering, University of Leeds, Leeds, LS2 9JT, United Kingdom, email: x.mao@leeds.ac.uk

Abstract

The main focus of this work is the optimization of a thermoacoustic plate stack in a standing-wave thermoacoustic refrigerator using genetic algorithm. A numerical model of the thermoacoustic stack and its iterative solving process are firstly presented. A comparison to DeltaEC modelling shows that the presented method is effective in predicting the acoustic field and the energy flow. Based on the numerical model, the stack is optimized in terms of four and five variables for both single objective and multiple objectives. In the four-variable models, the length and position of the stack, the plate spacing and the stack porosity are investigated. In the five-variable model, the acoustic frequency is considered additionally. In the single-objective optimization, the objective function is either the cooling power or the coefficient of performance of the stack, and the multi-objective model has two objective

* Corresponding author: Yehui Peng, email: pengyehui@hnust.edu.cn

functions, namely, the coefficient of performance of the stack and the cooling power. For the optimization, genetic algorithm hybridized by pattern search and implemented in Matlab is adopted. The optimal values of the stack length and the stack position, obtained from the single-objective optimization, agree with those in the published work. The extended multi-objective models present the Pareto optimal, which provides more design choices depending on the preference.

| Nomenclature | | | |
|---------------------|---|-------------------|---|
| P,p | Pressure (Pa) | π | 3.1415926... (-) |
| U | volumetric flow rate (m ³ -s) | ρ | Density(kg/m ³) |
| T | Temperature (K) | ω | angular frequency (s ⁻¹) |
| \dot{H} | total power (W) | γ | ratio of specific heat of gas (-) |
| \dot{E} | acoustic power (W) | σ | Prandtl number of gas (-) |
| COPs | coefficient of performance of the stack(-) | μ | Vicosity (kg/m.s) |
| i | imaginary unit (-) | $\delta_{k,v}$ | Thermal,viscous penetration depth (m) |
| A | Area (m ²) | ε_s | Correction factor for solid heat capacity (-) |
| Dr | driving ratio (-) | La | Spacing of stack= $2r_h/\delta_k$ (-) |
| Br | porosity or blockage ratio of the stack (-) | Subscripts | |
| $\Delta\dot{E}$ | Consumed acoustic power (W) | n | normalized value |
| x | Position (m) | 1 | first order acoustic variable |
| Re[] | Real part of (-) | 2 | Second order acoustic variable |
| | Magnitude of complex number (-) | s | stack |
| λ | wave length (m) | m | mean value |
| r_h | Hydraulic radius (m) | c | centre |
| a | speed of sound (m ⁻¹ s) | ref | reference parameter |
| L | Length (m) | a | Ambient end |
| ~ | Complex conjugate (-) | c | Cold end |
| f | Frequency (Hz) | gas | About gas |
| f_k | averaged thermal functions (-) | | |
| f_v | averaged viscous functions (-) | | |
| k | Thermal conductivity(W/mK) | | |

1. Introduction

Thermoacoustic refrigeration is an important application of thermoacoustic phenomenon, which is a kind of solid-fluid interaction that can facilitate heat pumping effect in working fluids. The thermoacoustic theory was not established until 1980s in a series of work by Rott^[1]. Further insights into thermoacoustic theory were provided by Xiao^[2] and Swift^[3].

Thermoacoustic refrigerators operate based on the fundamental principle where the acoustical work is used to pump heat from a low temperature reservoir to a high temperature one. The first successful thermoacoustic refrigerator was developed by Hofler^[4] in 1986. Since then, the thermoacoustic cooling technology has been considered a promising alternative to conventional ones. However, the existing thermoacoustic systems are generally characterized by their low performances^[5], which restrict their further developments and commercial applications^[6].

Another area of applications of thermoacoustic effect is thermoacoustic engines (or prime movers), by which thermal energy is converted to acoustic energy^{[7],[10]-[11],[12]}.

Both thermoacoustic engine and thermoacoustic refrigerator technologies still have many challenges to overcome for it to be more widely applied. At the centre of the challenges is an improved system efficiency. There have been many experimental and numerical investigations^{[13]-[29]} on various aspects affecting the system performance at both component and system levels.

Wetzel and Herman proposed an algorithm which serves as an easy-to-follow guideline for the design of thermoacoustic refrigerators^[13]. Babaei and Siddiqui developed a similar way to design thermoacoustically-driven thermoacoustic refrigerators^[14]. Piccolo presented a simplified computational method based on second law analysis to optimize the thermoacoustic refrigerator^[15].

Chen et al investigated the performance of an atmospheric pressure thermoacoustic cooling system by varying its operating frequency and obtained the optimal frequency range^[16]. The effects of working fluids and operating conditions, including temperature gradient in stacks, Prandtl number (Pr), driving ratio (Dr), and mean pressure (p_m), on the performance of thermoacoustic refrigerators were examined numerically^{[17]-[20]}. The effects of the stack position, length, plate spacing and thickness on the performance of thermoacoustic refrigerators were also scrutinized^{[18],[21]-[24]}. Zolpakar et al used multi-objective genetic algorithm to search for the optimum of four variables, which are the length and position of a stack, the blockage ratio and the driving ratio^[26]. DeltaEC, the numerical tool developed by Los Alamos National Laboratory, is particularly useful to help users to design thermoacoustic apparatuses to achieve desired performance with a good level of accuracy for low-amplitude thermoacoustic systems^[27]. Computational Fluid Dynamics is a potentially very useful tool to investigate thermoacoustic devices as demonstrated^{[28]-[29]}.

Optimization is one of the effective approaches to improve the performance of thermoacoustic refrigerators. For the thermoacoustic effects that take place in stacks, most of the optimization studies were done on the stacks^{[21]-[24],[26],[30]-[32]}. Most of the past experimental investigations were carried out in limited ranges of parameters and numerical optimization schemes were often constrained by the discrete variations of parameters to be optimized to achieve individual objectives^{[13]-[16],[18]-[21],[24]}. The outcome, therefore, could often be a local minimum/maximum. In order to find global optimum, various intelligent algorithms, including genetic algorithm^[23], particle swarm method^[31], machine learning^[32] and teaching-learning-based optimization algorithm^[30] have been applied to optimize the performance of the stack. Among all these attempts, the objective functions are all evaluated using the short-stack boundary layer approximation, which can be overly simple for practical design and can introduce errors to some degree to the optimum parameters. Nevertheless, attempts have been

made to combine DeltaEC with response surface method (RSM) to investigate the effect of the position and length of stacks on refrigerator performance^[30], albeit it is undeniable that there would be some error when the objective function is approximated by the response surface.

In this work, we developed a new approach for the modelling and optimization of a simple thermoacoustic refrigerator (TAR), more specifically, a thermoacoustic stack. We apply iterative solution to the weakly nonlinear thermoacoustic model^{[1]-[3]}, which better represents the underlying thermoacoustic effect than the short-stack approximation, and then integrate it with the optimization process based on genetic algorithm. The coupled numerical scheme is then used to optimize the parallel-plate stack in a standing-wave thermoacoustic refrigerator. The genetic algorithm is applied to simultaneously optimize the position of the stack in the resonator, the stack length, the plate spacing, and the porosity of the stack, as well as the operating frequency, while the cooling power and the coefficient of performance are chosen to be the objective functions. Heat exchangers are known to significantly contribute to reduced system performance. Due to their complex interactions with stacks in terms of both flow and heat transfer, they are neglected here in order to reduce the total number of independent variables for optimization.

2. Description of thermoacoustic models

Refs.[1]-[3] give a simplified thermoacoustic model, which have over 18 independent parameters that could affect the performance of a thermoacoustic system. The number of independent parameters can be reduced through normalization. Table 1 lists some of the independent parameters, and also in the table are the reference parameters represented by the subscript ref. Note that the reference frequency may not necessarily be the operating frequency.

Table 1 Normalization of Parameters

| Independent parameters | Normalizing parameters |
|------------------------|---|
| Length and position | $L_{ref} = \lambda_{ref}/2\pi$, where λ_{ref} is the wave length |
| Penetration depth | $y_{ref} = r_h$ |
| Pressure amplitude | $P_{ref} = P_m$ |
| Temperature difference | $T_{ref} = T_a$ |
| Area | $A_{ref} =$ Gas cross-section area at the ambient temperature end |
| Velocity | $a_{ref} =$ the speed of sound |
| Power | $W_{ref} = P_{ref} a_{ref} A_{ref}$ |
| Frequency | $\omega_{ref} = a_{ref}/L_{ref}$ |

After normalization, the thermoacoustics model presented in [1]-[3] can be expressed as follows:

$$\frac{dp_{1n}}{dx_n} = \frac{-i\gamma\omega_n}{(1-f_v)A_n T_{mn}} U_{1n}, \quad (1)$$

$$\frac{dU_{1n}}{dx_n} = \frac{-i\omega_n A_n}{\gamma} \left[1 + \frac{(\gamma-1)f_k}{1+\varepsilon_s} \right] p_{1,n} + \frac{f_k - f_v}{(1-f_v)(1-\sigma)(1+\varepsilon_s)} \frac{U_{1n}}{T_{mn}} \frac{dT_{mn}}{dx_n}, \quad (2)$$

$$\frac{dT_{mn}}{dx_n} = \frac{\dot{H}_{2n} - \frac{1}{2} Re \left[p_{1n} \tilde{U}_{1n} \left(1 - \frac{f_k - \tilde{f}_v}{(1-\tilde{f}_v)(1+\sigma)(1+\varepsilon_s)} \right) \right]}{\frac{\gamma}{2(\gamma-1)(1-\sigma)|1-f_v|^2} Im \left[\tilde{f}_v + \frac{(f_k - \tilde{f}_v)(1+\varepsilon_s f_v / f_k)}{(1+\varepsilon_s)(1+\sigma)} \right] \frac{|U_{1n}|^2}{\omega_n A_n T_{mn}} - \frac{T_{ref} k_{ref}}{L_{ref} P_{ref} a_{ref}} (A_n k_n + A_{sn} k_{sn})}. \quad (3)$$

$$\begin{aligned} \dot{H}_{2n} = & \frac{1}{2} Re \left[p_{1n} \tilde{U}_{1n} \left(1 - \frac{f_k - \tilde{f}_v}{(1-\tilde{f}_v)(1+\sigma)(1+\varepsilon_s)} \right) \right] \\ & + \frac{\gamma}{2(\gamma-1)(1-\sigma)|1-f_v|^2} Im \left[\tilde{f}_v + \frac{(f_k - \tilde{f}_v)(1+\varepsilon_s f_v / f_k)}{(1+\varepsilon_s)(1+\sigma)} \right] \frac{|U_{1n}|^2}{\omega_n A_n T_{mn}} \frac{dT_{mn}}{dx_n} \\ & - \frac{T_{ref} k_{ref}}{L_{ref} P_{ref} a_{ref}} (A_n k_n + A_{sn} k_{sn}) \frac{dT_{mn}}{dx_n} \end{aligned} \quad (4)$$

$$\dot{E}_{2,n} = \frac{1}{2} Re [p_{1n} \tilde{U}_{1n}] \quad (5)$$

The consumed acoustic power in the stack can be defined as

$$\Delta \dot{E}_{2,n} = \dot{E}_{2,n}(x_{cn} - 0.5L_{sn}) - \dot{E}_{2,n}(x_{cn} + 0.5L_{sn}). \quad (6)$$

Then the stack (COPs)^[13] is defined as

$$COPs = \frac{Cooling Power}{Consumed Power} = \frac{|\dot{H}_{2n}| - |\dot{E}_{2,n}(x_{cn} + 0.5L_{sn})|}{|\Delta \dot{E}_{2,n}|} \quad (7)$$

With acoustic approximation and assuming standing-wave phasing between pressure and velocity, the velocity and pressure can be expressed as^{[14],[18]}

$$p_{1n} = Dr \cos(\omega_n x_n), \quad U_{1n} = -\frac{iDr}{\gamma} \sin(\omega_n x_n). \quad (8)$$

In the short-stack approximation, the total power and the acoustic power (consumed or produced) in the stack are expressed as follows^{[3],[14]}

$$\dot{H}_{2n} \approx \frac{1}{8\gamma} \delta_{kn} Dr^2 \frac{\sin(2x_{cn})}{(1+\sigma)\Lambda} \left[\Gamma \frac{1+\sqrt{\sigma}+\sigma}{1+\sqrt{\sigma}} - (1 + \sqrt{\sigma} - \delta_{vn}) \right] \quad (9)$$

$$\Delta \dot{E}_{2n} \approx \frac{\delta_{kn} Dr^2 L_{sn} Br}{4\gamma} \left[(\gamma - 1) \cos^2(x_{cn}) \left(\frac{\Gamma}{(1+\sqrt{\sigma})\Lambda} - 1 \right) - \frac{\sin^2(x_{cn}) \sqrt{\sigma}}{Br^2 \Lambda} \right] \quad (10)$$

where $\Lambda = 1 - \delta_v/r_h + \delta_v^2/2r_h^2$. The normalized temperature gradient Γ is expressed as^[18]

$$\Gamma = \frac{\Delta T_{mn}}{Br(\gamma-1)L_{sn} \cot(x_{cn})}$$

3. Numerical Method

This section will develop a coupled iterative process that integrates the calculation of acoustic field and power with an optimization algorithm to optimize the thermoacoustic refrigerator.

3.1 Calculation of Acoustic Field and Power in Stacks

For given stack geometries and working fluids, there are four variables, p_{1n} , U_{1n} , T_{mn} and \dot{H}_{2n} in the thermoacoustic equations (1)-(3). Assume the outer walls of the resonator are adiabatic, so the working media in the stack will have no heat exchange with the external reservoir. Then in the stack we have

$$\frac{\dot{H}_{2n}}{dx} = 0 \quad \text{or} \quad \dot{H}_{2n} = \text{const} \quad (11)$$

Equations (1)-(3) and (11) together form a differential system that will be closed under suitable boundary conditions. Standing-wave phasing is assumed between the pressure and the velocity in the resonator and the effect of heat exchanger on the acoustic field negligible.

We have the following boundary conditions on the left end of the stack:

$$p_{1n}(x_{cn} - 0.5L_{sn}) = Dr \cos(\omega_n(x_{cn} - 0.5L_{sn})), \quad (12)$$

$$U_{1n}(x_{cn} - 0.5L_{sn}) = \frac{-iDr}{\gamma Br} \sin(\omega_n(x_{cn} - 0.5L_{sn})). \quad (13)$$

Additionally, the mean temperature should satisfy the following temperature boundary conditions

$$T_{mn}(x_{cn} - 0.5L_{sn}) = T_{an}, \quad (14)$$

$$T_{mn}(x_{cn} + 0.5L_{sn}) = T_{cn}. \quad (15)$$

Then the above boundary conditions (12)-(15) close the system (1)-(3) and (11). However, this system is not a standard boundary value problem. Common approaches for differential systems, such as Runge-Kutta method, cannot be used directly. A different efficient algorithm is needed.

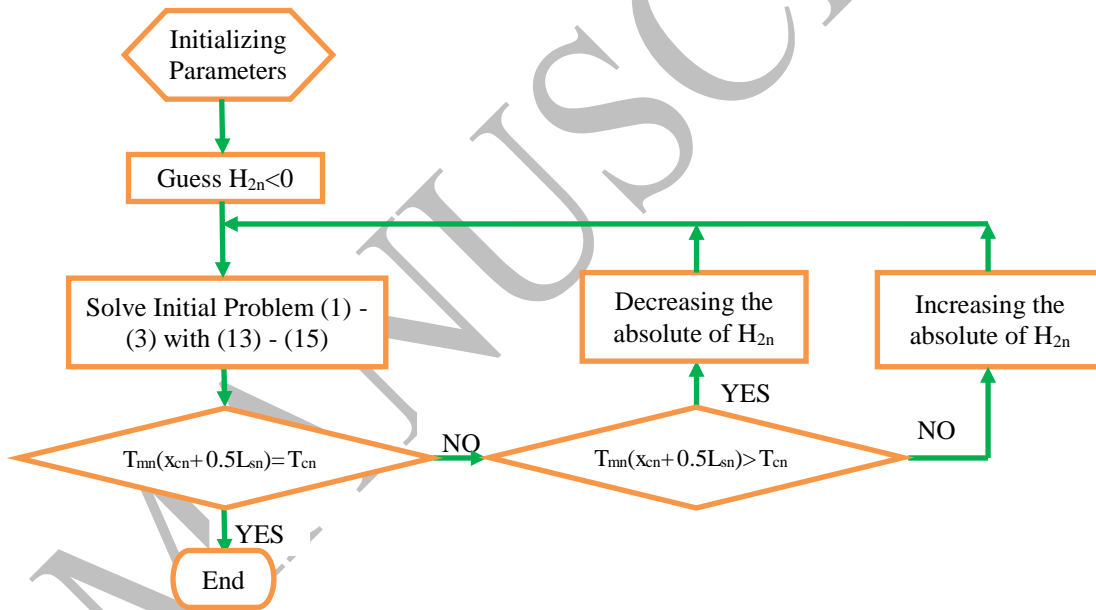


Fig. 1 Flow chart of calculation of acoustic field in standing wave thermoacoustic stacks

Since \dot{H}_{2n} is constant in the stack, the above system can be treated as a standard boundary value problem, which includes equations (1)-(3) and (12)-(14), mixed with an algebra equation (11). One can iteratively search for \dot{H}_{2n} such that the solutions to the system of

equations (1)-(3) and (12)-(14) satisfy the boundary condition (15). This iteration process is different from the shooting algorithm used in DeltaEC and can be illustrated using the flow chart given in Fig.1.

3.2 Optimization of stacks

For the design and operation of refrigerators, one may pursue a maximal cooling power for small scale devices, for instance^[36]. Therefore, it is intuitive to select cooling power as the objective function. The single-objective optimal model hence has the objective as follows,

$$\text{Max } \{\text{Cooling Power}\}.$$

From the effectiveness point of view, one expects the performance of the stack, in terms of coefficient of performance (COPs) for instance, to be as high as possible. This is particularly desirable for large scale devices^[36]. So one may maximize the COPs, that is,

$$\text{Max } \{\text{COPs}\}$$

Moreover, one may expect to maximize the COPs and the cooling power simultaneously. Then the following multi-objective optimization can satisfy the goal.

$$\text{Max } \{\text{COPs, Cooling Power}\}.$$

As we know, COPs and the cooling power are usually conflicting with each other, which can be seen from Fig. 5 in Ref.[18]. In both simple- and multi-objective models given above, the objective functions will be evaluated using the algorithm presented in Section 3.1. In the investigation of the effects of the stack geometry and the driving condition on the efficiency and the cooling power, the variables include x_{cn} , sL_{sn} , Br , $La = 2r_h/\delta_k = 2\delta_{kn}$ and operating frequency (ω_n).

Next, the constraints on the variables need to be determined. Generally, stacks should be located between a pressure antinode and a pressure node, and the thermoacoustic effect is

strong near the pressure antinode. If the stack is too short, the cooling power will be very small^[18] and the refrigeration could even be lost in the extreme. Furthermore, it has been shown that the COPs becomes highly sensitive to the stack length when $L_{sn} < 0.9$, which is disadvantageous to the practical design^[18]. Therefore the following constrains of the position and length of stack are being considered.

$$x_{cn} - \frac{L_{sn}}{2} \geq 0, \quad x_{cn} + \frac{L_{sn}}{2} \leq \frac{\pi}{2\omega_n}$$

$$0.09 \leq L_{sn} \leq \frac{\pi}{2}$$

It has also been pointed out that the stack should be separated by a distance between $2\delta_k$ and $4\delta_k$ ^{[5],[13]}. So the range of stack spacing is set as

$$1 \leq La \leq 5$$

As for the porosity, it should not be too small and doesn't exceed 1. From a practical point of view, the range of porosity is set as

$$0.5 \leq Br \leq 0.95$$

There are few published works seen to have investigated the effect of operating frequency. This is partly due to the fact that the short-stack approximation model, which uses Eqs. (9)-(10), is not explicitly related to the operating frequency. To have a compact resonator and a high power density, a high frequency is often preferred. It also results in possible reduction in acoustic power dissipation in the stack due to the decrease in the viscous penetration depth, although the resulted small stack spacing desirable poses a challenge to the fabrication of the stack. The small displacement amplitude as a result of a high operating frequency also increases the difficulty in installing efficient heat exchangers. An operating frequency (f) of 400 Hz was chosen in the experimental investigation and optimization for standing-wave refrigerators^{[14],[18],[23]}. Wetzel and Herman adopted the operating frequency of 325 Hz for the TALSR under examination^[13]. In this work ω_{ref} is set as $2\pi \times 400$ rad/s is chosen to enable a

comparison with the results in the literature. To investigate the effect of the operating frequency, the angular frequency is considered in the interval as follows:

$$0.01 \leq \omega_n \leq 1.8$$

4. Validation

4.1 A case study

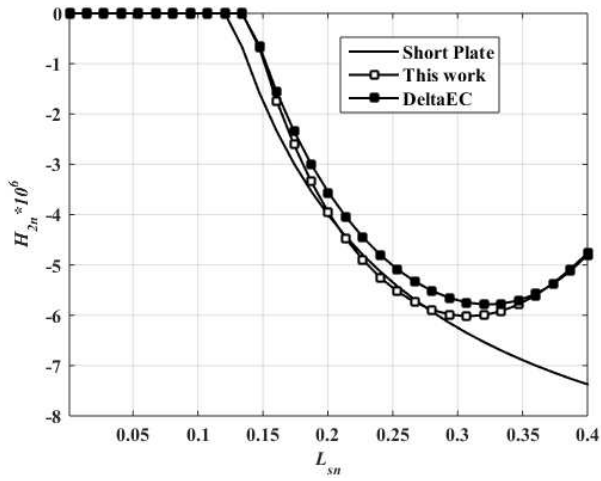
In order to validate the method described above and to demonstrate its advantage over the short-stack boundary layer approximation, a comparison is made between this method and the short-stack boundary layer approximation, as well as DeltaEC, for the following case^[18]. Table 2 lists the operation parameters and the properties of the working fluid.

Table 2 Operating Parameters, Working Fluid Properties and Stack Material

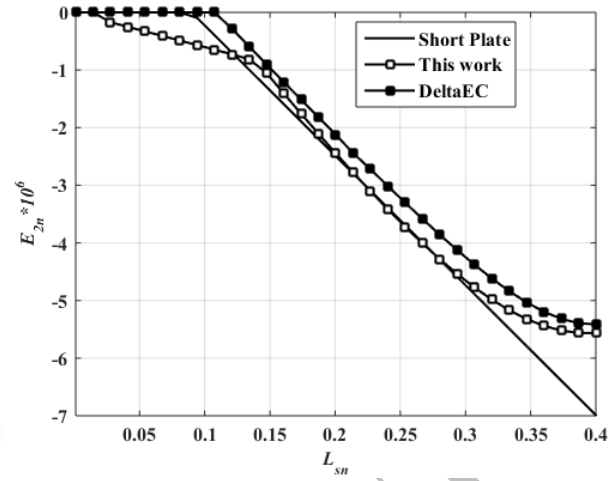
| Operation Parameters | Working Fluid Properties | Stack Material |
|----------------------|-------------------------------------|-------------------------------------|
| $p_m=10\text{bar}$ | Helium | $k_s=0.16\text{W/mK}$ |
| $T_a=287.5\text{K}$ | $a=937.7\text{ m/s}$ | $\rho_s=10201\text{kg/m}^3$ |
| $T_c=212.5\text{K}$ | $\sigma=0.68$ | $\text{Br}=0.75$ |
| $\text{Dr}=0.02$ | $\gamma=1.67$ | $L_s=0.091302\text{m}$ |
| $f=400\text{Hz}$ | $k=0.1479\text{ W/mK}$ | $x_c=0.0873\text{m}$ |
| | $\mu=1.9369\text{e-}5\text{ kg/ms}$ | Spacing $3.4896\text{e-}4\text{ m}$ |

When normalized, L_{ref} is 0.39697m , and the normalized stack length and the position are $L_{\text{sn}} = 0.23$ and $x_{\text{cn}} = 0.22$, respectively. Additionally, the spacing $La = 3.0$ and $\omega_n = 1$.

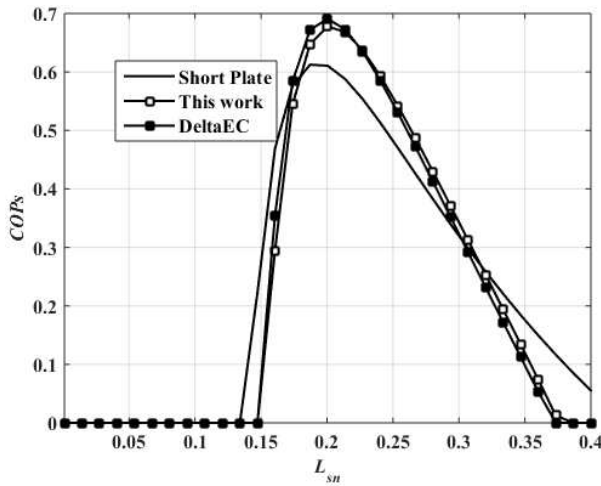
Figure 2 shows the results of the non-dimensional H_{2n} , E_{2n} , COPs and cooling power calculated using the short-stack boundary layer approximation, our method and DeltaEC, respectively. The centre of the stack is fixed at 0.22 from the left end of the thermoacoustic refrigerator.



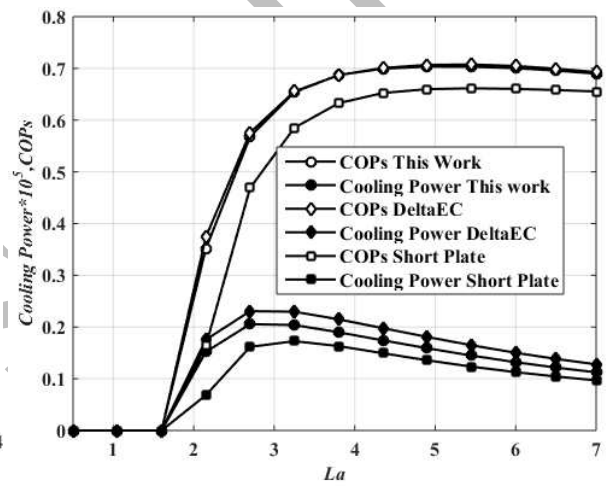
(a)



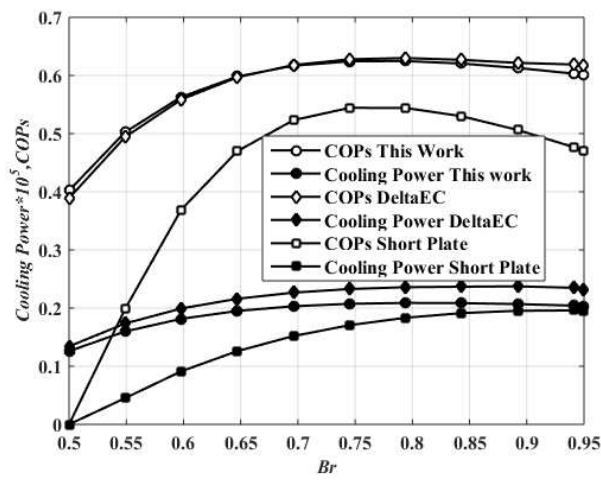
(b)



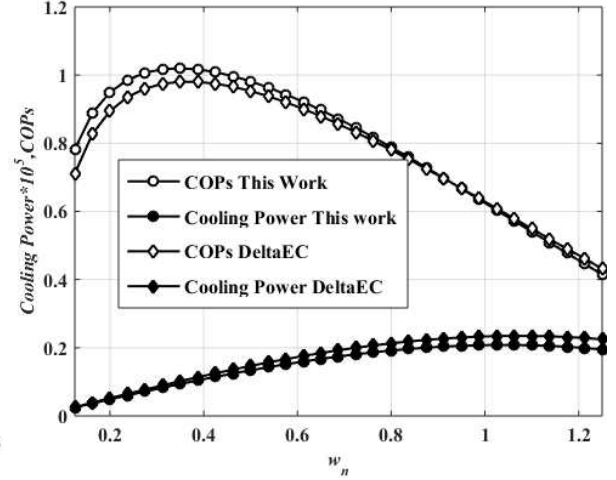
(c)



(d)



(e)



(f)

Fig.2 The comparison of this work with DeltaEC and the short-stack approximation shows the variations of (a) H_{2n} , (b) E_{2n} and (c) COPs as the stack length changes, and the variations of COPs and cooling power as a function of (d) spacing L_a , (e) porosity and (f) operating frequency.

Figures 2(a), 2(b) and 2(c) describe the variations of H_{2n} , E_{2n} and COPs, respectively, with the changing stack length. When the stack length, L_{sn} , is very small, the short stack will lead to a great temperature gradient, when the temperature difference over the stack remains constant as in this case. If the normalized temperature gradient exceeds some critical value, the stack will operate in the engine mode, and heat flow is along the temperature gradient and net acoustic power is produced. So the values of H_{2n} , E_{2n} will be positive or zero. As this work focuses on the standing-wave refrigerator, H_{2n} , E_{2n} and COPs are assigned zero to indicate a positive or zero total power flux in (a), a net acoustic power production in (b) and no cooling power in (c), respectively.

The short-stack boundary layer approximation predicts that when $L_{sn} \leq 0.134$, $L_{sn} \leq 0.0941$ and $L_{sn} \leq 0.1473$ there are $H_{2n} = 0$, $E_{2n} = 0$ and $COPs = 0$, respectively. The corresponding normalized temperature gradients (dT/dx) are 0.8707, 1.2399 and 0.7921, respectively. In comparison, both our method and DeltaEC give $L_{sn} \leq 0.1473$, $L_{sn} \leq 0.1207$ and $L_{sn} \leq 0.1606$ for $H_{2n} = 0$, $E_{2n} = 0$ and $COPs = 0$, respectively, and the corresponding normalized temperature gradients are 0.7921, 0.9666 and 0.7265, respectively. This means that the short-stack boundary layer approximation predicts a critical temperature gradient a little greater than that our method and DeltaEC give. Moreover, when the stack length L_{sn} is greater than 0.3, the discrepancies in H_{2n} , E_{2n} and COPs become greater between the short-stack boundary layer approximation and DeltaEC, and eventually even the trends are no longer similar. When $L_{sn} > 0.31$, H_{2n} from the short-stack boundary layer approximation is monotonically increasing with the stack length, whereas the values of H_{2n} from our method and DeltaEC are monotonically decreasing. When $L_{sn} > 0.3734$, both our

method and DeltaEC give zero COPs, while the short-stack boundary layer approximation provides a non-zero COPs. Furthermore, our method and DeltaEC give a maximum COPs at $L_{sn} = 0.2005$, but the short-stack boundary layer approximation predicts a maximum COPs at $L_{sn} = 0.1872$.

Figure 2(d) describes the variation of COPs and cooling power as a function of the stack spacing L_a . All three methods reveal the nonlinear varying trends of COPs and cooling power with an increasing stack spacing. Our method gives almost the same L_a - COPs curve as DeltaEC and a rather similar L_a - cooling-power curve. However, the short-stack approximation gives results of a greater difference from that of DeltaEC. This confirms that our method can correctly predict COPs and cooling power in the examined range of stack spacing L_a .

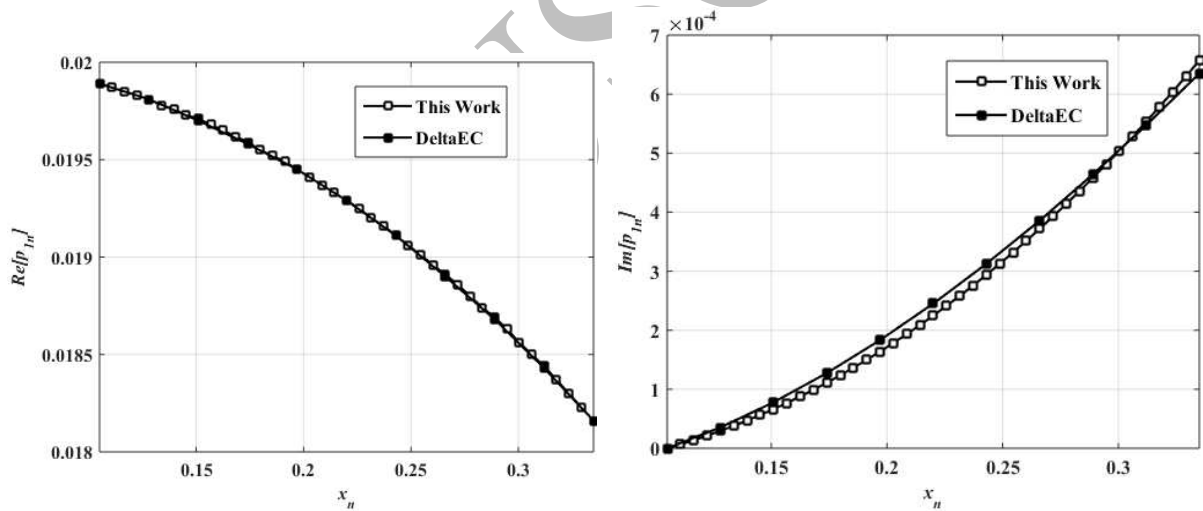
Figure 2(e) displays variations of COPs and cooling power with the porosity. It clearly shows the difference between the values of COPs and cooling power from the short-stack approximation and those from DeltaEC. It is also clear to see that our method has nearly the same output as DeltaEC. The maximal differences between the presented method and DeltaEC are 0.0154 in COPs and 2.785×10^{-7} in cooling power, respectively, while using the short-stack approximation the minimal absolute differences are 0.08348 in COPs and 3.609×10^{-7} in cooling power, respectively. This further demonstrates that the present method is able to give more accurate output than the short-stack approximation method.

Figure 2(f) depicts the variation of COPs and cooling power with the operating frequency. Since the short-stack approximation does not consider the effect of operating frequency, a comparison is only made between the present method and DeltaEC, which shows almost the same results of COPs and cooling power from both our model and DeltaEC. The maximum discrepancy is 0.07136 in COPs occurring at a low frequency of $\omega_n = 0.25$ and the maximum

discrepancy in cooling power is 2.981×10^{-7} at a high frequency of $\omega_n = 1.25$. In addition, it is clearly evident that, the frequency presents completely different effects on COPs and cooling power in that the COPs reaches its maximum at low frequencies and the cooling power has a maximum at high frequencies. Therefore, this figure once more confirms that the present method has a similar capability to DeltaEC of providing the output required.

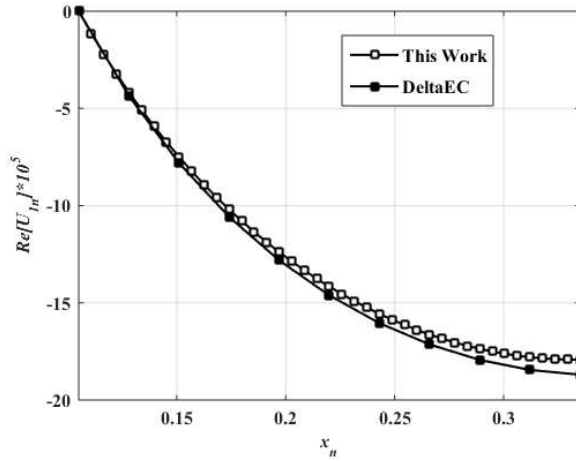
4.2 Acoustic field and temperature distribution in a stack

Figure 3 gives the distributions of p_{1n} , U_{1n} and T_{mn} in the stack, calculated using the presented method and DeltaEC under the operation conditions listed in Table 2. It is clear to see that the two methods give nearly same p_{1n} , U_{1n} and T_{mn} distributions. The maximum difference between the values of p_{1n} , U_{1n} and T_{mn} given by the presented method and DeltaEC is less than 4%, which occurs to $\text{Re}[U_{1n}]$ at the right end of the stack.

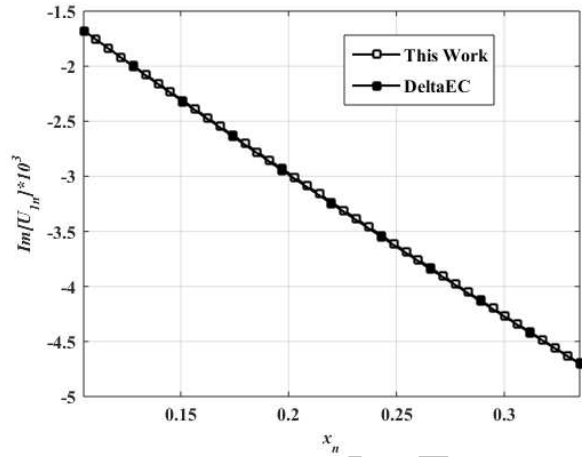


(a) Distribution of $\text{Re}[p_{1n}]$ in the stack

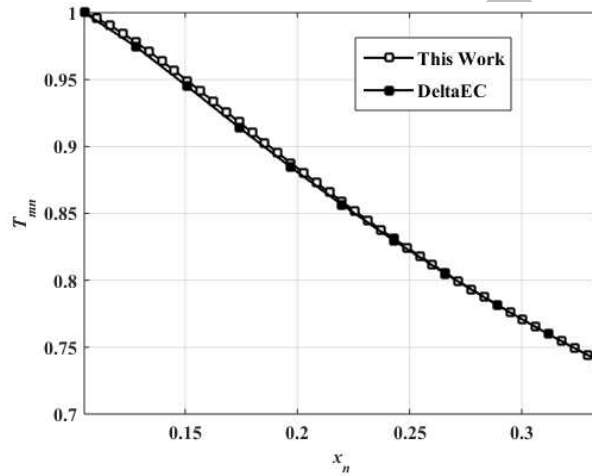
(b) Distribution of $\text{Im}[p_{1n}]$ in the stack



(c) Distribution of $\text{Re}[U_{1n}]$ in the stack



(d) Distribution of $\text{Im}[U_{1n}]$ in the stack



(e) Distribution of T_{mn} in the stack

Fig.3 Distribution of p_{1n} , U_{1n} and T_{mn} in the stack

It can be concluded that the presented method is more accurate than the short-stack boundary layer approximation for the case under investigation, and it is comparable to DeltaEC in the ability to predict the acoustic field in the stack. It can also be seen that the parameters such as the stack position, the stack length, the plate spacing, the stack porosity and the operating frequency can affect COPs and cooling power. In the following section, we investigate their effects in details, by incorporating the presented iterative method into optimization process.

5. Optimization Results and Discussion

As can be seen, the objective functions are highly nonlinear and they do not have analytic solutions. Also the evaluation of objective functions is an iterative numerical process, so it is unfeasible to use high-order algorithms, such as the Newton Method, to optimize the thermoacoustic system. As mentioned earlier in Section 1, several artificial intelligence algorithms were able to realize global optimization, with only the evaluation of objective function necessary. Among these algorithms, the genetic algorithm has been successfully utilized in the area of thermoacoustic optimization^{[5],[22],[23]}, which shows its attractive capability.

In this work, due to the high probability to find the global maxima, the strong robustness and the lack of need for explicit formula for the objective function, we chose to apply the genetic algorithm in Matlab^[34] to optimize thermoacoustic stacks. The main parameters of the genetic algorithm are listed in Table 3, and other parameters are set as default in Matlab. The optimization was carried out on a desktop PC equipped with two Intel Core i5-6500 processors (3.20GHz and 3.19GHz) and 4GB of RAM and Window 10 OS. The operating conditions are the same as those in Table 2, except the design variables, including stack position x_{cn} , stack length L_{sn} , plate spacing La , porosity Br and operation frequency ω_n . Parallel-plate stacks are considered in this work.

Table 3 Parameters of Genetic Algorithm

| Parameter | Value |
|--------------------|----------------------|
| Population size | 50 |
| Generation | 800 |
| Crossover Fraction | 0.8 |
| Elite count | 0.05*Population Size |
| TolCon | 1.0e-8 |

In the four-variable model, the stack length, centre position, porosity and spacing are included. In the five-variable model, the operating frequency is also included, in order to investigate the effect of operating frequency on the COPs and cooling power.

5.1 Results of Single-Objective Models

Because of the randomness of the genetic algorithm, the genetic algorithm function in Matlab is called 30 times continuously to find the best solution to single-objective models. Results were obtained of both single-objective models, namely the model maximizing cooling power and the model maximizing the coefficient of performance of the stack. For convenience, the models maximizing cooling power and COPs are referred as MMCP and MMCOP hereafter, respectively.

5.1.1 Results from Model Maximizing Cooling Power (MMCP)

After 6188s and 6802s, we obtain the output of four- and five-variable models, respectively.

The output of four-variable model shows that the third call of the genetic algorithm for the four-variable model gives the highest normalized cooling power of $2.127e-06$, when the stack length $L_{sn} = 0.248$, the stack spacing $La = 2.923$, the stack position $x_{cn} = 0.253$, and the porosity $Br = 0.943$ (the shaded row). The corresponding COPs is 0.557. Under the same conditions, DeltaEC predicts a normalized cooling power of $2.416e-6$ and a COPs of 0.573. These values are close to those obtained by Zolpakar et al ^[23], where the best normalized cooling power was predicted to be $1.6e-6$, when the stack length $L_{sn} = 0.24$ and the stack position $x_{cn} = 0.22$ under the condition of a fixed stack spacing $La = 3$ and a porosity $Br = 0.75$. Between our results and those from Zolpakar et al ^[23], the differences in the stack length and the stack position are about 3% and 15%, respectively. The short-stack approximation was used by Zolpakar et al ^[23], which is suspected to be the cause of the difference. The high

porosity obtained using our method is caused by the omission for simplification of heat transfer process in the solid. In practice, the porosity of stacks will be much lower.

The result of five-variable model informs that the maximum normalized cooling power can be obtained is $2.233e-06$, slightly higher than that obtained from four-variable single-objective MMCP model, when the operating frequency is additionally examined in the single-objective optimization. The stack length, the stack spacing, the stack position, the porosity and the operating frequency are $L_{sn} = 1.561$, $L_a = 2.907$, $x_{cn} = 1.310$, $Br = 0.601$ and $\omega_n = 0.156$, respectively. There is also $COPs = 0.594$, also slightly higher than obtained from four-variable single-objective MMCP model. Under the same condition, DeltaEC gives a normalized cooling power of $2.297e-6$ and a $COPs$ of 0.606 . The optimal dimensional frequency is 62.4Hz (0.156×400). This different frequency from the reference value of 400Hz is the result of a local optimum of the performance of the stack alone when the frequency is subject to vary. In comparison, the design in Ref. [18] started from a choice of a high frequency for the benefit of a high power density and possibly a compact acoustic resonator. Extending the results above, we think it is important to optimize, if possible, the operating frequency when the whole refrigerator is being considered.

At first sight, the results of four-variable model and those of five-variable model are different. If one examines the length and the position of stacks in relation to the wavelength specific to individual cases, it can be seen they are indeed similar to each other. Before arriving at this point, we first consider the relative length and position to the wavelength defined as follows

$$\frac{L_s}{\lambda/2\pi} = \frac{L_s}{L_{ref}} \frac{\lambda_{ref}}{\lambda} = L_{sn}\omega_n, \quad \frac{x_c}{\lambda/2\pi} = \frac{x_c}{L_{ref}} \frac{\lambda_{ref}}{\lambda} = x_{cn}\omega_n$$

Here we use the fact that the acoustic velocity is independent of frequency, so $\lambda_{ref}/\lambda = \omega/\omega_{ref} = \omega_n$. In the four-variable model $\omega_n \equiv 1$. Thus we have

$$\left(\frac{L_s}{\lambda/2\pi}\right)_{(opt,4)} = (L_{sn}\omega_n)_{(opt,4)} = 0.248329, \quad \left(\frac{x_c}{\lambda/2\pi}\right)_{(opt,4)} = (x_{cn}\omega_n)_{(opt,4)} = 0.253137,$$

$$\left(\frac{L_s}{\lambda/2\pi}\right)_{(opt,5)} = (L_{sn}\omega_n)_{(opt,5)} = 0.243686, \quad \left(\frac{x_c}{\lambda/2\pi}\right)_{(opt,5)} = (x_{cn}\omega_n)_{(opt,5)} = 0.204496.$$

The notation $(a)_{(opt,i)}$ denotes that it is the optimal value of a parameter a of the i -variable model. It is shown above that the optimal stack length and position relative to the specific wavelength of the two models are nearly same.

To summarise, the optimal values of the stack length and the stack position, the stack spacing and the porosity are about 0.24, 0.21, 2.9 and 0.61, respectively, obtained using the model maximizing cooling power. These optimal results agree with those seen in Refs. [18], [23] and [26].

5.1.2 Results of Models Maximizing COPs (MMCOP)

It took 37107 seconds and 50349 seconds, respectively, to obtain the outputs of four- and five-variables MMCOP.

The optimal stack length, position, spacing and porosity for four variable MMCOP are 0.109, 0.143, 3.17 and 0.950, respectively. Moreover, the optimal values for five-variable MMCOP are 1.083, 1.571, 2.076, 0.950 and 0.024, respectively, where the value 0.024 is the optimal frequency.

Comparing the results of four- and five-variable MMCOP, one will find that the driving frequency affects the COPs greatly, similar to what we can observe in Section 5.1.1. The output of four-variable MMCOP informs that the maximum COPs is only 1.030 when the driving frequency is set as 400Hz. When the driving frequency is 9.8Hz ($\omega_n = 0.024$), a greater COPs at 1.656 can be obtained.

The optimal values clearly show that MMCP and MMCOP give different outputs. This matches with our expectation that the objectives of maximum cooling power and maximum COPs are usually in conflict with one another. Similar conclusion can also be seen in Ref. [35].

The optimal normalized stack length (L_{sn}) obtained from MMCP is greater than that from MMCOP in both four- and five-variable cases. This is due to the different behaviour in the change of the enthalpy and work fluxes following the change of stack length^[7, 13]. The work flux tends to increase proportionally with the stack length due to the linear relationship between the viscous loss and the total surface area. Whereas, the enthalpy flux contributing to the cooling power increases firstly quickly, and the increase becomes less until the stack length reaches a critical value when the cooling power diminishes^[7]. As a result, the maximum COPs normally appears with a smaller stack length, and the maximum cooling power requires a slightly longer stack.

For four-variable MMCP and MMCOP, the optimal porosity (Br) are 0.943 and 0.950, respectively. And the optimal Br for five-variable MMCP and MMCOP are 0.601 and 0.950, respectively. It seems that MMCOP gets its maximum at the maximal Br, no matter what the frequency is. With the four-variable MMCP, i.e. the working frequency is fixed at 400 Hz, the optimal porosity has a high value of 0.943. When the frequency can be lowered, the optimal porosity can be significantly reduced (to 0.601), which is more realistic from a practical point of view. The different requirement for the stack length and the stack position, the porosity and the spacing to achieve maximum cooling power and COPs can be more clearly seen using multi-objective optimization in the following section, for both a fixed frequency and a varied one.

5.2 Results of Multi-Objective Model

The multi-objective genetic algorithm function in Matlab is called 10 times continuously. It took 7924s and 9513s to reach the Pareto solution set for the four- and five-variable multi-objective models, respectively. As mentioned earlier, the two objectives, namely COPs and cooling power, are in conflict with one another. As a result, the multi-objective optimization gives Pareto optimal. The Pareto solution sets of four- and five-variable models are shown in Fig.4. Comparing results of multi-objective model with those of single-objective model, we can find that the maximum cooling powers in the Pareto solution sets is nearly the same as the optimal solutions obtained from the corresponding single-objective models. This indicates the consistence of our model in providing promising optimized results.

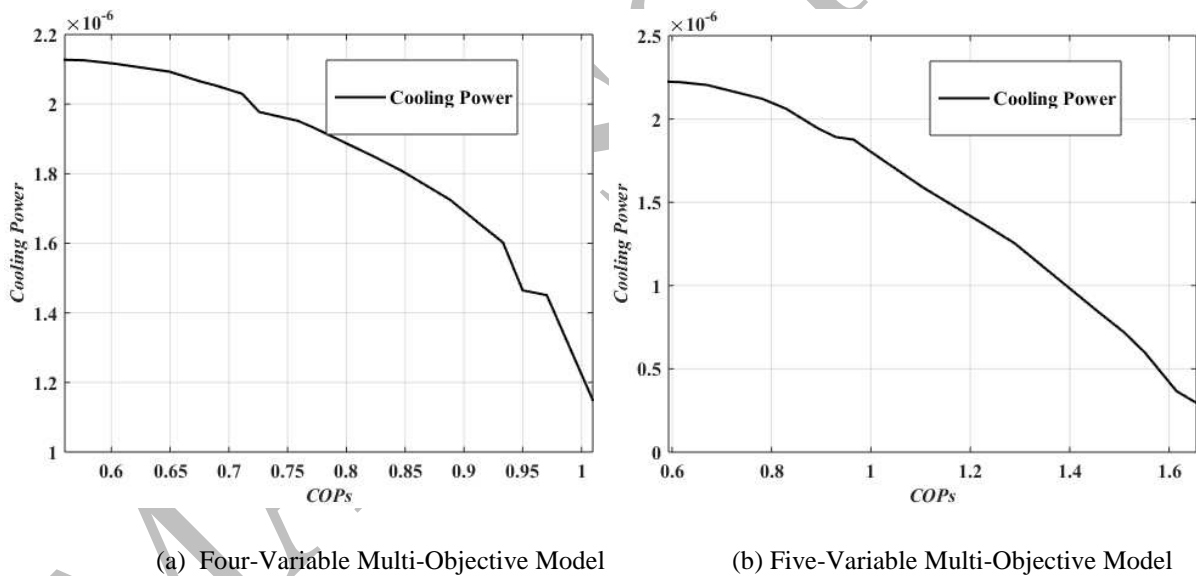


Fig. 4 Pareto front of cooling power versus COPs from the multi-objective model

As shown by Fig.4, the quadrant has been divided into two regions by the solid line representing the Pareto front. In theory, one can achieve a design of the thermoacoustic stack as long as the desirable cooling power and COPs is to the left-bottom of the Pareto front indicated by the solid curves. The Pareto optimal represents the maximum cooling power achievable for a given COPs or the best COPs at certain cooling power level. It is evident that

the multi-objective model can provide more design choices. As it can also be seen from the difference between Figs. 4a and 4b that, the operating frequency has significant effect on the COPs and cooling power in that both the maximum COPs and cooling power from the five-variable model are greater than those from the four-variable model. It is also interesting to see from Fig. 4 that the Pareto fronts appear to have two asymptotes which may represent the maximal cooling power and COPs respectively, even though the exact values of the asymptotes are not directly confirmed from the ten solution sets.

6. Conclusions

This work presents an iterative algorithm for the determination of the acoustic field and heat flow in a stack in standing-wave thermoacoustic refrigerators. The method provides the possibility to be integrated with an optimization algorithm to look for an optimal configuration of stacks in thermoacoustic refrigerators.

By imbedding our method of solving the nonlinear thermoacoustic equations into a genetic algorithm, the integrated models are numerically solved using the genetic algorithm in Matlab. The results show that the single-objective four- and five-variable models give optimal parameters consistent with those in published works. With single-objective MMCP, the optimum stack length and position, relative to the specific wavelength, are about 0.24 and 0.21, respectively, according to the five-variable model. The optimal stack spacing, porosity and frequency are about 2.9, 0.6 and 62Hz, respectively. Additionally, a lower optimal frequency has been predicted in this work, which considers the stack only. In comparison, with the five-variable single-objective MMCOP, the optimal relative stack length and the stack position, the stack spacing, porosity and frequency are 0.038, 0.026, 2.076, 0.950 and 9.8Hz. The multi-objective models successfully identify the Pareto fronts which represent the

limit of cooling power for any given values of COPs and the maximum COPs at certain cooling power level. Clearly, the multi-objective models provide more design possibilities.

Acknowledgement

This work is supported financially by National Natural Science Foundation of China (No. 51476052). Y Peng and H Feng are grateful to Professor Artur J. Jaworski and Faculty of Engineering, University of Leeds for the host and hospitality, when they were visiting the Thermoacoustics Group and conceived the main idea of this work.

MANUSCRIPT

Reference

- [1] N Rott. Thermoacoustics Advances in Applied Mechanics 1980, 20: 135-175
- [2] J H Xiao. Thermoacoustic heat transportation and energy transformation Part 1: Formulation of the problem. Cryogenics 1995, 35(1): 15-19.
- [3] G W Swift. Thermoacoustics: a unifying perspective for some engines and refrigerators. The Acoustical Society of America, NY: Melville; 2002.
- [4] T J Hofler. Thermoacoustic refrigerator design and performance, PhD.thesis. San Diego: Physics Department, University of California; 1986.
- [5] Nor Atiqah Zolpakar, Normah Mohd-Ghazali, Mawahib Hassan El-Fawal. Performance analysis of the standing wave thermoacoustic refrigerator: A review, Renewable and Sustainable Energy Reviews 2016, 54:626–634
- [6] M E Poese, W M Robert, S L Garret. Thermoacoustic refrigeration for ice cream sales. Journal of Acoustical Society of America 2004, 107(5):2480–6.
- [7] S Backhaus and G W Swift. A thermoacoustic-Stirling heat engine: Detailed study. The Journal of the Acoustical Society of America 2000, 107, 3148
- [8] M E H Tijani and S Spoelstra. A high performance thermoacoustic engine. Journal of Applied Physics 2011, 110, 093519
- [9] S Backhaus, E Tward and M Petach. Traveling-wave thermoacoustic electric generator. Applied Physics Letters 2004, 85(6), 1085-1087
- [10] Ahmed Hamood, Artur J. Jaworski, Xiaoan Mao, Kevin Simpson. Design and construction of a two-stage thermoacoustic electricity generator with push-pull linear alternator. Energy 2018, 144, 61-72
- [11] J A Mumith, C Makatsoris, T G Karayiannis. Design of a thermoacoustic heat engine for low temperature waste heat recovery in food manufacturing: A thermoacoustic device for heat recovery. Applied Thermal Engineering 2014, 65(1–2), 588-596
- [12] Zhanghua Wu, Wei Dai, Man Man, Ercang Luo. A solar-powered traveling-wave thermoacoustic electricity generator. Solar Energy 2012, 86(9), 2376-2382
- [13] M Wetzel, C Herman. Design optimization of thermoacoustic refrigerators. International Journal Refrigeration 1997, 20:3–21.
- [14] Hadi Babaei, Kamran Siddiqui, Design and Optimization of Thermoacoustic Devices, Energy Conversion and Management, 2008, 49: 3585–3598

- [15] A Picollo. Optimization of thermoacoustic refrigerators using second law analysis. *Applied Energy* 2013, 103:358–67.
- [16] B Chen, Abakr Yousif Abdalla, Al-Atabi Mushtak. Investigation of an atmospheric pressure thermoacoustic cooling system by varying operating frequency. *Journal of Engineering Science and Technology* 2013, 83:364–71.
- [17] C Jensen, R Raspet, W Slaton. Temperature gradient integration in thermoacoustic stacks. *Applied Acoustic* 2006, 67:689–699.
- [18] M E H. Tijani, J C H. Zeegers, A T A M. De Waele. Design of thermoacoustic refrigerators *Cryogenics* 2002, 42: 49-57
- [19] A Campo, M M Papari, E Abu-Nada. Estimation of minimum Prandtl number for binary gas mixtures formed with light helium and certain heavier gases: application to thermoacoustic. *Applied Thermal Engineering* 2011, 31:3142–3146.
- [20] S H Tasnim, S Mahmud, R A Fraser. Effect of variation of working fluid and operating conditions on the performance of thermoacoustic refrigerator. *International Communication of Heat and Mass Transfer* 2012, 9:762–768.
- [21] F Wu, L Chen, A Shu, X Kan, K Wu, Z Yang. Constructal design of stack filled with parallel plates in standing-wave thermosacoustic cooler. *Cryogenics* 2009, 49:107–111.
- [22] N A Zolpakar, N M Ghazali, R Ahmad. Analysis of increasing the optimized parameters in improving the performance of a thermoacoustic refrigerator. *Energy Procedia* 2014, 61:33–36.
- [23] Nor Atiqah Zolpakar, Normah Mohd-Ghazali, and Robiah Ahmad. Optimization of the Stack Unit in a Thermoacoustic Refrigerator, *Heat Transfer Engineering* 2017, 38(4): 431-437
- [24] N M Hariharan, R Sivashanmugam, S Kasthuriengan. Influence of stack geometry and resonator length on the performance of thermoacoustic engine. *Applied Acoustic* 2012, 73:1052–1058.
- [25] D W Zhang, Y L He, W W Yang, Y Wang, W Q Tao. Particle image velocimetry measurement on the oscillatory flow at the end of thermoacoustic parallel stacks. *Applied Thermal Engineering* 2013, 51:325–333.
- [26] N A Zolpakar, N M Ghazali, R Ahmad. Simultaneous optimization of four parameters in stack unit of a thermoacoustic refrigerator. *International Journal of Air-Conditioning and Refrigeration* 2014, 22(2):1450011.

- [27] J P Clark, W C Ward, G W Swift. Design environment for low-amplitude thermoacoustic energy conversion (DeltaEC), *The Journal of the Acoustical Society of America* 2007, 122(5): 3014.
- [28] Mathew Skaria, K K Abdul Rasheed, K A Shafi, S Kasthuriangan, UpendraBeher. Simulation studies on the performance of thermoacoustic prime movers and refrigerator, *Computers & Fluids* 2015, 111(16): 127-136
- [29] A Namdar, A Kianifar, E Roohi. Numerical Investigation of thermoacoustic refrigerator at weak and large amplitudes considering cooling effect. *Cryogenics* 2015, 67:36–44.
- [30] A B Desai, K P Desai, H B Naik and M D Atrey. Optimization of thermoacoustic engine driven thermoacoustic refrigerator using response surface methodology, *IOP Conf. Series: Materials Science and Engineering* 2017, 171: 012132
- [31] H Chaitou, P Nika. Exergetic optimization of a thermoacoustic engine using the particle swarm optimization method. *Energy Conversion and Management* 2012, 55:71–80.
- [32] Jurriath-Azmathi Mumith, Tassos Karayiannis, Charalampos Makatsoris. Design and optimization of a thermoacoustic heat engine using reinforcement learning, *International Journal of Low-Carbon Technologies* 2016, 11(3):431-439
- [33] Ravipudi Venkata Rao, Kiran Chunilal More, Jan Taler & Pawel Ocloń. Multi-objective optimization of thermo-acoustic devices using teaching-learning-based optimization algorithm, *Science and Technology for the Built Environment* 2017, 23:8, 1244-1252.
- [34] Using the Genetic Algorithm, *Global Optimization Toolbox User's Guide*, MATLAB R2015a, The MathWorks, Inc, MA, US
- [35] L.K. Tartibu, B. Sun, M. A. E. Kaunda. Lexicographic multi-objective optimization of thermoacoustic refrigerator's stack, *Heat Mass Transfer* 2015, 51:649–660
- [36] C. Herman, Z. Travnicek. Cool sound: the future of refrigeration? Thermodynamic and heat transfer issues in thermoacoustic refrigeration. *Heat and mass transfer* 2006, 42(6), pp.492-500.